> Banner appropriate to article type will appear here in typeset article

Scaling and mechanism of the propagation speed of the upstream turbulent front in pipe flow

Haoyang Wu[1], and Baofang Song[2]†

[1]Center for Applied Mathematics, Tianjin University, Tianjin 300072, China

[2]State Key Laboratory of Turbulence and Complex system, College of Engineering, Peking University, Beijing 100871, China

Scaling and mechanism of the propagation speed of turbulent fronts in pipe flow with the Reynolds number has been a long-standing problem in the past decades. Here, we derive an explicit scaling law of the upstream front speed, which approaches to a power-law scaling at high Reynolds numbers, and explain the underlying mechanism. Our data show that the average wall distance of low-speed streaks at the tip of the upstream front, where transition occurs, appears to be constant in local wall units in the wide bulk-Reynolds-number range investigated, between 5000 and 60000. By further assuming that the axial propagation of velocity fluctuations at the front tip, resulting from streak instabilities, is dominated by the advection of the local mean flow, the front speed can be derived as an explicit function of the Reynolds number. The derived formula agrees well with the measured speed by front tracking. Our finding reveals a relationship between the structure and speed of a front, which enables to obtain a close approximation of the front speed based on a single velocity field without having to track the front over time.

1. Introduction

Front formation and propagation are important processes in nonlinear systems involving reaction, diffusion and advection, such as combustion, neural systems, epidemics and turbulent flows. In pipe flow, a localized turbulent region expands via the propagation of the upstream front (UF) and downstream front (DF) into the laminar region, where the flow is stable to infinitesimal perturbations (Meseguer & Trefethen 2003; Chen *et al.* 2022*b*). See FIG. 1 for an illustration. The front speeds determine the expansion rate of the turbulent region and consequently the wall friction. Therefore, front speed is an important characteristic of pipe flow turbulence and, together with the front structure, has been the subject of many studies in the past six decades (Lindgren 1957, 1969; Wygnanski & Champagne 1973; Darbyshire

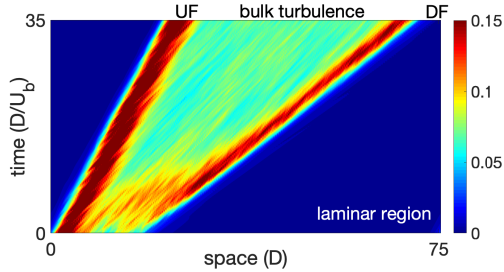† Email address for correspondence: baofang.song@pku.edu.cn

Abstract must not spill onto p.2

Figure 1: The expansion of a turbulence at $Re = 5000$. Contours of the magnitude of transverse velocity (averaged over the pipe cross-section) are plotted in the space (pipe axis) and time plane. The length unit in space is pipe diameter D and time unit is D/U_b with U_b being the bulk speed of the flow. The main stream is from left to right, and time is vertically up. Red color shows highly turbulent and blue color shows laminar regions. Different slopes of the two red stripes (fronts) indicate different front speeds, i.e. the turbulent region expands.

& Mullin 1995; Shan *et al.* 1999; Durst & Ünsal 2006; Nishi *et al.* 2008; van Doorne & Westerweel 2008; Duguet *et al.* 2010; Holzner *et al.* 2013; Barkley *et al.* 2015; Barkley 2016; Song *et al.* 2017; Rinaldi *et al.* 2019; Wang & Goldenfeld 2022; Chen *et al.* 2022*a*). Yet the mechanism that determines the front speed and the scaling of the speed with the Reynolds number (Re) remains largely unclear to date.

Most relevant studies focused on the narrow regime of transition from localized puffs to expanding turbulent states, i.e. slugs, at relatively low Reynolds numbers of $O(10^3)$. Due to difficulties of measuring front speed at high Re (Chen *et al.* 2022*a*), especially for the DF, only Wygnanski & Champagne (1973) and Chen *et al.* (2022*a*) considered higher Re at $O(10^4)$. Reasonable agreement has been obtained among existing measurements for the UF speed, showing a monotonically decreasing trend as Re increases (see Chen *et al.* (2022*a*) and Avila *et al.* (2023) for a latest literature review). However, Wygnanski & Champagne (1973) and Chen *et al.* (2022*a*) reported opposite speed trends above $Re \simeq 10000$ for the DF. By direct numerical simulations (DNS) up to $Re = 10^5$, Chen *et al.* (2022*a*) reported fits $\tilde{c}_{UF} = 0.024 + (Re/1936)^{-0.528}$ for the UF and $\tilde{c}_{DF} = 1.971 - (Re/1925)^{-0.825}$ for the DF, and argued for the monotonic trends of the two front speeds with Re at high Reynolds numbers. Although fitting the measured speeds well, these are pure data fits with a prescribed form but the underlying mechanism was left unexplained. In these fits and throughout this paper, the reference length and velocity are pipe diameter D and bulk speed U_b, respectively. The Reynolds number is defined as $Re = U_b D/\nu$ where ν is the kinematic viscosity. We will only consider the UF speed in this work.

Other than direct measurements of the front speed by tracking the front along the pipe axis, as in most studies, a few theoretical attempts have been made. For example, based on an energy flux analysis of the front region, without considering the dynamic transition process, Lindgren (1969) predicted an asymptotic speed of 0.69 as $Re \to \infty$. However, this prediction was questioned by both experimental (Wygnanski & Champagne 1973) and numerical (Chen *et al.* 2022*a*) measurements, which showed much lower speeds than the asymptotic prediction of Lindgren (1969). Barkley *et al.* (2015) and Barkley (2016) used a theoretical model to investigate the front in the transitional regime, which captures the large-scale dynamics of the fronts successfully. The asymptotic analysis explains the front speed as a combination of the advection of the bulk turbulence and a propagation with respect to the bulk turbulence (see FIG. 1). However, as a generic model for one-dimensional reaction-

diffusion-advection systems, the model does not account for the three dimensionality of the transition for pipe flow and does not give an explicit relationship between the front speed and Re. Besides, the Re range considered was too narrow for a scaling with Re to be established. Similar problems apply to the stochastic prey-predator model recently proposed by Wang & Goldenfeld (2022) which nevertheless can reproduce the basic phenomenology of the front of pipe flow in the transitional regime. In a word, there is still a big gap between experiments and theory.

In this paper, our goal is to derive a scaling law of the front speed by accounting for the transition at the front.

2. Results

Our starting point is the observation of our earlier work (Chen *et al.* 2022*a*) that transition to turbulence continuously occurs at the tip of a front (see supplementary movie), maintaining a characteristic propagation speed and a characteristic shape of the front against the distortion of the mean shear. For an upstream front, the front tip refers to its upstream-most point. We propose that an evaluation of the radial position of the transition point at the front tip is crucial for determining the front speed. The questions are how to quantitatively determine this position and relate it to the front speed.

Before presenting our results, the setup of the flow system and some notations should be explained. The flow is incompressible and constant-mass-flux driven, and is solved in cylindrical coordinates, where (r, θ, z) denote radial, azimuthal and axial coordinates, respectively, and u_r, u_θ, and u_z denote the respective fluctuating velocity components in the three directions. The axial length of the pipe domain is $17.5D$ for $Re \leqslant 10000$ and $5D$ for higher Re. The readers are referred to Chen *et al.* (2022*a*) for more details about the simulation of a front in a short periodic pipe.

We first show the flow structure at the tip of the UF. In figure 2(a), contours of the magnitude of transverse velocity fluctuation in the $z - r$ plane show that turbulence is concentrated near the wall and gradually spreads out toward the pipe center while going downstream (see the online movie for more details). Figure 2(b) shows the distribution of maximum $|u_z|$ and $|u_r|$ in the $r - \theta$ crosssection along the pipe axis. These curves also reflect that the flow is nonturbulent on the upstream side of the front tip and turbulent on the downstream side. Figure 2(c) shows that the flow features nearly straight and streamwise-elongated low-speed (blue) and high-speed (red) streaks on the upstream side, whereas the flow structure is less regular on the downstream side of the front tip. These plots (especially figure 2b) suggest that the tip of the UF should sit in the interval $z \in (3, 3.5)$ roughly. Figure 2(d) shows the contours of u_z in the $r - \theta$ plane at $z = 3.18$. Alternating high-speed (red spots) and low-speed streaks (blue spots) can be seen close to the wall, while the flow is laminar in the core region of the pipe.

Although there still lacks a quantitative description of the transition mechanism at the UF tip, the consensus seems to be that the transition is caused by instabilities of the low-speed streaks (Shimizu & Kida 2009; Duguet *et al.* 2010; Hof *et al.* 2010) (which may consist of more fundamental substructures according to Jiang *et al.* (2020*a*,*b*)). The instabilities here possibly coincide with those (either modal or nonmodal) proposed for explaining either subcritical transition or the self-sustaining mechanism of shear flow turbulence (Swearingen & Blackwelder 1987; Hamilton *et al.* 1995; Zikanov 1996; Waleffe 1997; Schoppa & Hussain 1998, 2002; Meseguer 2003).
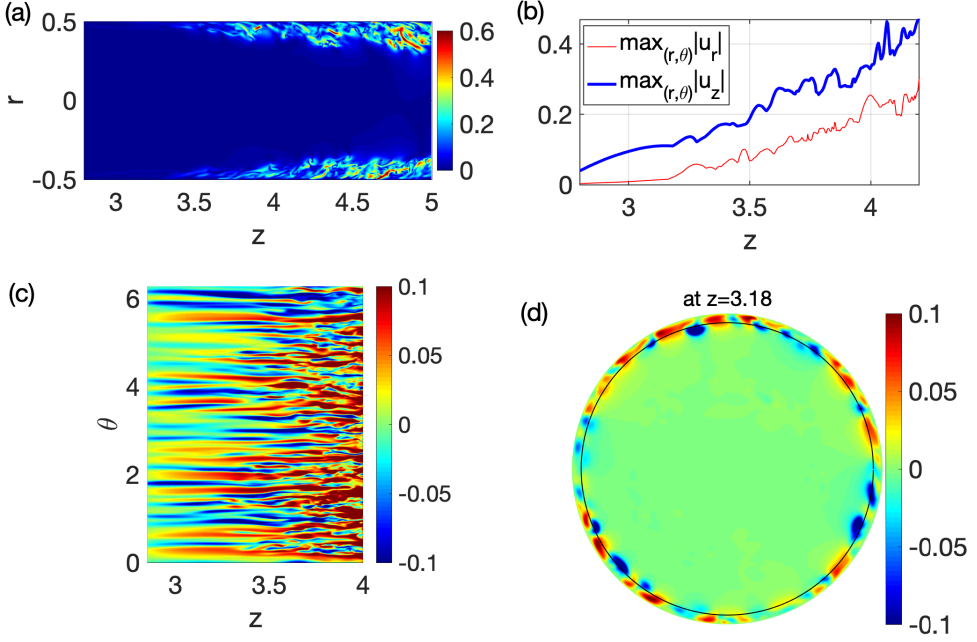
Figure 2: Structure of a UF. (a) The tip part (the upstream-most part) of a UF in a $z - r$ plane at $Re = 40000$. Contours of the transverse velocity $\sqrt{u_r^2 + u_\theta^2}$ are plotted in the $z - r$ crosssection. The main flow is from left to right, and blue region is low-velocity-fluctuation region and red region is high-velocity-fluctuation region. (b) The maximum of $|u_r|$ and $|u_z|$ in the $r - \theta$ crosssection plotted along the pipe axis. (c) Contours of u_z in the $z - \theta$ plane at $r = 0.47$, which show low-speed (blue) and high-speed (red) streaks. (d) Contours of u_z in the $r - \theta$ crosssection at $z = 3.18$. The circle, at $r = 0.47$, shows the radial position of the $z - \theta$ plane in panel (c). This circle approximately shows the average position of low-speed streaks (blue spots) at this axial position.

In the following, we will establish a connection between the low-speed streaks and the front speed based on a few hypotheses, the first of which reads

H1 *The wall distance of transition point at the front tip, in local wall unit, is independent of the Reynolds number statistically.*

This should be reasonable because the transition takes place near the wall so that the wall distance of the transition point can be expected to scale with the wall length, which is the only length scale that can be derived from viscosity and wall shear. We will verify this hypothesis by measuring the wall distance of low-speed streaks as a proxy of that of the transition point.

At a turbulent front, the flow is axially developing so that low speed streaks are not parallel to the pipe wall but oblique, i.e. the wall distance varies along a streak. Figure 3(a,b) suggest that low-speed streaks are gradually lifted up away from the wall while going downstream. To more quantitatively show this variation, we take the following approach to determine the wall distance of low-speed streaks at a given axial location. In an $r - \theta$ cross-section, low-speed streaks can be detected by setting a proper threshold in u_z, and regions enclosed by contour lines of the specified threshold can be considered as (the cross-sections of) low-speed streaks, see the magenta contour lines in Fig. 3(a) with a threshold -0.04. See Appendix
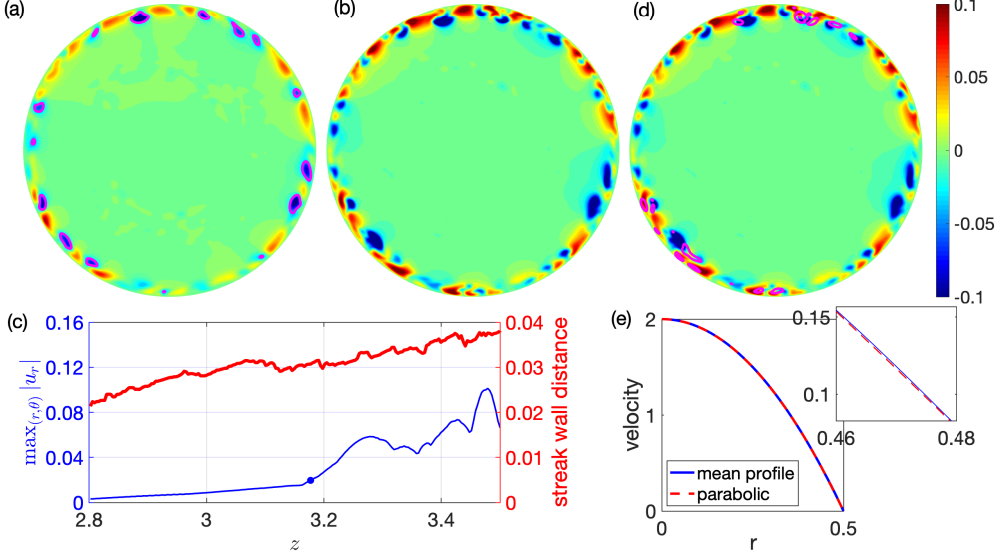
Figure 3: Axial variation of the low-speed streaks (a-d) and mean velocity profiles near the front tip (e). The flow field is the same as that shown in FIG. 2. (a) Contours of u_z at $z = 3.0$. The contour level of -0.04 is plotted in magenta color to highlight the low-speed streaks. (b) Contours at $z = 3.3$. (c) The variation of the average wall distance of streaks (bold red) and $\max_{(r,\theta)} |u_r|$ (thin blue) along the pipe axis. (d) Also at $z = 3.3$, and the contour level 0.025 of the transverse velocity $\sqrt{u_r^2 + u_\theta^2}$ is plotted in magenta color to highlight the transverse velocity fluctuations. (e) The mean velocity profile at $z = 3.3$, i.e. $U(r) = < u_x(r, \theta, 3.3) >_\theta$, where $< \cdot >_\theta$ means average in the azimuthal direction. The parabolic profile is plotted as a broken line for comparison. The small window highlights the deviation between the two in the near wall region
.

135   A for a discussion on the threshold selection. Then, the nominal wall distance of a
136   streak can be defined as the wall distance of the minimum of u_z within the streak.
137   The average wall distance is calculated as the arithmetic mean of the wall distances
138   of all the streaks detected in this pipe cross-section. Fig. 3(c) more quantitatively
139   shows that the wall distance of streaks increases as going downstream. Therefore, it
140   is necessary to determine the axial position of the front tip for finally determining the
141   wall distance of the streaks at the front tip. We use $\max_{(r,\theta)} |u_r|$, which is a function
142   of z, as an indicator of the local flow state. This curve is smooth and slowly varying
143   in the laminar region and wiggles around in turbulent region, see Fig. 2(b) and Fig.
144   3(c). The axial location of the front tip can be estimated by the position separating
145   the smooth and wiggling parts of the curve of $\max_{r,\theta} |u_r|$. We use an algorithm that
146   detects abrupt changes of a curve for this purpose, which is built-in as the function
147   *findchangepts* in MATLAB R2018a (see Appendix B for a brief description of the
148   algorithm). The blue dot in Fig. 3(c) shows the separating point determined using
149   this algorithm.
150   Figure 4(a) shows the average wall distance of streaks $y = 0.5 - r$ at the front tip
151   in outer units. The larger the Re, the smaller the y, which can be expected. Figure
152   4(b) shows y^+, the wall distance in local wall length unit $\sqrt{\nu/\tau_w}$, where τ_w is the
153   local wall shear stress. Considering that the azimuthally averaged velocity profiles at
154   these axial locations are nearly parabolic (see FIG. 3e), τ_w is simply approximated
155   by the value of the parabolic profile. It appears that y^+ stays nearly constant in the
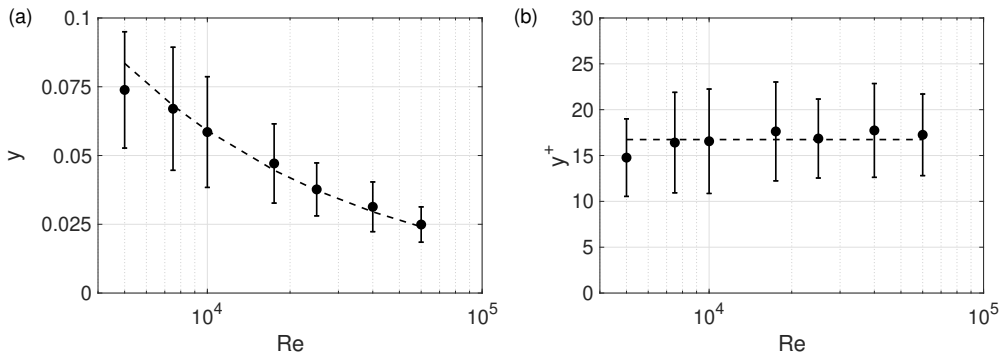
Figure 4: The average wall-distance of the low-speed streaks at the tip of the UF. (a) The distance in the outer length unit. (b) The distance in the local wall unit. At each Re, about 10 to 20 velocity snapshots are collected, giving 100 to 200 low-speed streaks approximately for the statistics. The standard deviation is plotted as the errorbar. The dashed lines are equation (2.1) by taking $A = 16.7$, which is the average of y^+ over all Re shown in panel (b)

.

wide Re range considered, which supports our hypothesis H1 given the crucial role that low-speed streaks play in the transition.

Assuming this Re-independence, we derive the scaling law of the speed of the UF as following. Taking the wall distance of the transition point at the front tip to be $y_F^+ = A$, where A is independent of Re. Then, in outer units, we have

$$y_F = y_F^+/Re_\tau = A/Re_\tau. \tag{2.1}$$

The local mean flow speed, i.e. the azimuthally-averaged streamwise velocity at the radial position of the transition point, in outer units, can be approximated by the local laminar value

$$U(y_F) \approx 2 - 8\left(0.5 - y_F\right)^2 = 8\left(A/Re_\tau - A^2/Re_\tau^2\right), \tag{2.2}$$

given that the mean velocity profile is nearly parabolic at the front tip. As the relationship between Re and Re_τ is

$$Re_\tau = \sqrt{-\frac{\mathrm{d}U(r)}{\mathrm{d}r}\Big|_{r=0.5}Re} \quad = 2\sqrt{2Re} \tag{2.3}$$

for a parabolic velocity profile, we have

$$U(y_F) \approx 2\sqrt{2}ARe^{-0.5} - A^2Re^{-1}. \tag{2.4}$$

Now it comes to our further hypotheses:

H2 *The wall distance of velocity perturbations at the front tip, resulting from streak instabilities, can be closely approximated by the wall distance of the streaks.*

H3 *The front speed is determined by the axial propagation speed of these velocity perturbations, which approximately equals the local mean flow speed.*

H2 should be reasonable, especially when perturbations appear at the flanks of the streaks. In fact, the data seems to support this hypothesis, see FIG. 3(d) where most of the strong-perturbation region, enclosed by magenta contour lines, seems to be at the flanks of the low-speed streaks. H3 is based on our presumption that streak instabilities generate streamwise vortices, which further generate streaks while being advected downstream, seeding new transition and closing the self-sustaining
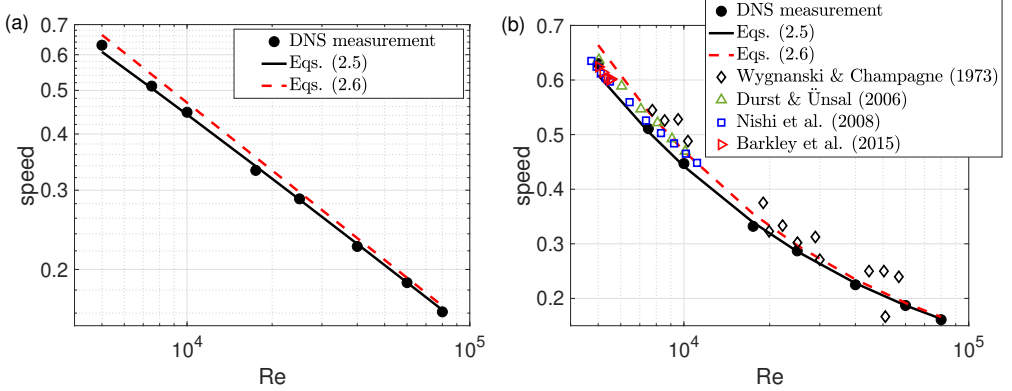
Figure 5: Comparison of derived and measured front speeds. The circles show the speeds measured by front tracking using DNS (Chen *et al.* 2022*a*). The solid black line shows the approximation Eqs. (2.5) with $A = 16.7$, which is the average of the y^+ (black circles in FIG. 4b) over all Re's. The dashed red line shows the approximation Eqs. (2.6) with $A = 16.7$ also. Panel (b) is the same plot in linear scale for the speed where some data sets from the literature falling in this Re range are also included.

182 cycle of the dynamics at the front tip. Therefore, the propagation speed of these
183 vortices likely determines that of the front tip and consequently the front speed. The
184 propagation of vortical structures, at least in fully developed wall turbulence above
185 the viscous sublayer, was shown to be dominated by the advection of the local mean
186 flow (Del Álamo & Jiménez 2009; Pei *et al.* 2012; Wu & Moin 2008).
187   Following these hypotheses, we finally have an approximation of the front speed
188 as

$$c_{UF} \approx U(y_F) \approx 2\sqrt{2}ARe^{-0.5} - A^2Re^{-1}, \tag{2.5}$$

190 and an asymptotic approximation at large Re

$$c_{UF} \approx U(y_F) \approx 2\sqrt{2}ARe^{-0.5}, \tag{2.6}$$

192 where A can be approximated by the wall distance of low-speed streaks at the front
193 tip.
194   Figure 5 concludes the speed measurements and our derivation. The filled circles
195 are the DNS data from Chen *et al.* (2022*a*) (up to $Re = 60000$) and the open symbols
196 show the literature data in the Re range investigated here. In order to show that the
197 formula is predictive, DNS at $Re = 80000$ is performed here, and the front speed
198 is measured by front tracking and plotted as a filled circle also. The black solid line
199 shows our derivation (2.5) by setting $A = 16.7$, which is the average of y^+ of streaks
200 at all Re's as shown in figure 4b. The relative error of the prediction is on the level
201 of a few percent compared to the DNS measurement. The red dashed line shows the
202 asymptotic speed (2.6) with the same A. Some former experimental measurements
203 are also included in the figure. It should be noted that this formula can also be
204 considered as a model for the front speed with only one parameter A, which has a
205 physical meaning and, more precisely, should be interpreted as the wall distance of
206 the transition point at the front tip. This formula can be used for other Re's after
207 calibrating the parameter A at one Re with the measured front speed.
208   Now we revisit the fit $\tilde{c}_{UF} = 0.024 + (Re/1936)^{-0.528}$ by Chen *et al.* (2022*a*).
209 This was obtained by assuming a form of $a + bRe^\beta$ without an explanation of
210 the underlying physics. In other words, this form is not unique. Besides, the small

constant 0.024 implies that the front speed would not approach zero as Re approaches infinity, which was unexplained and seems counter-intuitive. It is probably just a result of measurement errors and the specific prescribed form of the fit. In contrast, our derivation (2.5) makes no assumption on the specific form of the formula. It follows naturally from the dynamics we observed at the front tip with a few hypothetical but reasonable assumptions of the physics.

Our derivation (2.5) may suffer larger errors at lower Re. The low-speed streaks would be larger in transverse size at lower Re, therefore, the position of a streak estimated simply by the position of the minimum of u_z in each streak becomes less representative. Besides, the streak position may not exactly coincide with the position of velocity fluctuations resulting from the streak instability. But these positions are close to each other at sufficiently high Re so that our derivation will be more accurate.

As for the DF, the front speed is probably determined by the advection of the local mean flow at the front tip also. However, transition to turbulence occurs close to the pipe center (Chen *et al.* 2022a) and the transition may not be triggered by streak instabilities as known for near-wall turbulence. Therefore, the location of the transition point may not scale with the wall length unit, and cannot be explicitly related to Re as shown here for the UF at the present. This problem has to be left for future studies.

3. Conclusions

In summary, the speed of the UF of pipe flow turbulence was derived as an explicit function of Re based on the dynamics at the front tip. To our knowledge, this is the first of such since the seminal measurements and theoretical analysis of Lindgren (1957, 1969) about six decades ago. The agreement with speed measurements (see FIG. 5) suggests that the mechanism proposed here captures the core of the physics, i.e. the front speed is largely determined by the advection of velocity fluctuations by the local mean flow at the front tip where transition takes place. This mechanism may also apply to turbulent fronts in other shear flows where turbulence propagates into subcritical laminar flow region. Although the local mean flow is different in higher dimensions such as planar shear flows (see, e.g. Duguet & Schlatter (2013); Tao *et al.* (2018); Tuckerman *et al.* (2020); Klotz *et al.* (2021)), our work will be helpful for elucidating the physics of front propagation in those flows.

Appendix A. Threshold for detecting streaks

The results presented in the main text takes the threshold of -0.04. Here we explain the selection of this value. Figure 6 shows the contour levels of -0.02, -0.04 and -0.06 in the $r - \theta$ crosssection at $z = 3.18$ (the same position as shown in FIG
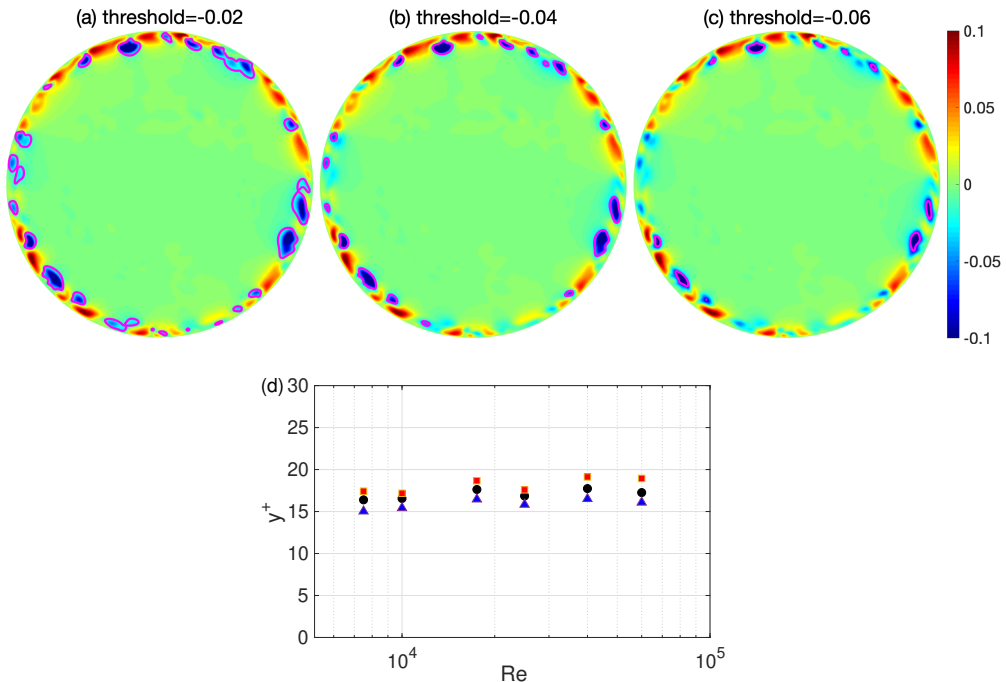
Figure 6: Thresholds for detecting low-speed steaks. Contours of streamwise velocity fluctuation in the $r - \theta$ crosssection for $Re = 40000$ as also shown in FIG. 2 of the main text. Contour levels of -0.02, -0.04 and -0.06 are plotted as magenta lines. (d) The average wall distance of low-speed streaks in wall units determined with thresholds of -0.02 (blue triangles), -0.04 (black circles) and -0.06 (red squares) in u_z for detecting the streaks.

2(d) of the main text), plotted as magenta lines. It can be seen that -0.02 cannot very well separate adjacent streaks, whereas -0.06 may miss out many streaks. We checked multiple velocity snapshots and Reynolds numbers and found it is often the case. The threshold -0.04 is a reasonable choice because, in most cases, it separates streaks well and is able to detect most of low-speed streaks.

It can be expected that the value of this threshold will affect the average position of the streaks. A higher threshold may drop out weaker streaks and only retain stronger streaks. Stronger streaks are often more lifted up away from the wall (can be seen in Figure 6), and therefore, a higher threshold will give a larger average wall distance of the streaks. Here we measured the average wall distance y^+ of the streaks determined using thresholds -0.02 and -0.06, see the blue triangles and the red squares, respectively, in Figure 6(d). It can be seen that -0.02 gives slightly lower and -0.06 gives slightly higher y^+ compared to the black circles (with a threshold of -0.04 for detecting streaks). But the important point is that the y^+ also appears to be a constant in the Re range considered using either threshold for detecting the streaks.

Appendix B. The algorithm for determining the axial location of the front tip

In the main text, we use the algorithm that is built in as the function *findchangepts* in MATLAB to detect abrupt changes in a signal sequence $[x_1, x_2, ..., x_n]$. The key

is to minimize the following target function

$$J(k) = \sum_{i=1}^{k-1} \left(x_i - \text{mean}([x_1, x_2, ..., x_{k-1}])\right)^2 + \sum_{i=k}^{n} \left(x_i - \text{mean}([x_k, x_{k+1}, ..., x_n])\right)^2$$

(B 1)

by modifying the index k. The resulted k is regarded as the separation point of the slowly-varying and abruptly varying-parts of the sequence. The data sequence of $\max_{r,\theta} |u_r|$, containing both the laminar part and turbulent part on the upstream and downstream sides of the front tip, respectively, is fed as the input. The output will be taken as the point separating the laminar part and turbulent part of the curve, which we define as the axial location of the front tip. The readers are referred to the documentation of MATLAB (version R2018a) for more details about the algorithm.

REFERENCES

AVILA, M., BARKLEY, D. & HOF, B. 2023 Transition to turbulence in pipe flow. *Ann. Rev. Fluid Mech.* **55**, 575–602.

BARKLEY, D. 2016 Theoretical perspective on the route to turbulence in a pipe. *J. Fluid Mech.* **803**, P1.

BARKLEY, D., SONG, B., MUKUND, V., LEMOULT, G., AVILA, M. & HOF, B. 2015 The rise of fully turbulent flow. *Nature* **526**, 550–553.

CHEN, K., XU, D. & SONG, B. 2022*a* Propagation speed of turbulent fronts in pipe flow at high Reynolds numbers. *J. Fluid Mech.* **935**, A11.

CHEN, Q., WEI, D. & ZHANG, Z. 2022*b* Linear stability of pipe Poiseuille flow at high Reynolds number regime. *Comm. Pure Appl. Math.* **76**, 1868–1964.

DARBYSHIRE, A. G. & MULLIN, T. 1995 Transition to turbulence in constant-mass-flux pipe flow. *J. Fluid Mech.* **289**, 83–114.

DEL ÁLAMO, J. C. & JIMÉNEZ, J. 2009 Estimation of turbulent convection velocities and corrections to Taylor's approximation. *J. Fluid Mech.* **640**, 5–26.

VAN DOORNE, C. W. H. & WESTERWEEL, J. 2008 The flow structure of a puff. *Phil. Trans. R. Soc. A.* **367**, 489–507.

DUGUET, Y. & SCHLATTER, P. 2013 Oblique laminar-turbulent interfaces in plane shear flows. *Phys. Rev. Lett.* **110**, 034502.

DUGUET, Y., WILLIS, A. P. & KERSWELL, R. R. 2010 Slug genesis in cylindrical pipe flow. *J. Fluid Mech.* **663**, 180–208.

DURST, F. & ÜNSAL, B. 2006 Forced laminar to turbulent transition in pipe flows. *J. Fluid Mech.* **560**, 449–464.

HAMILTON, J. M., KIM, J. & WALEFFE, F. 1995 Regeneration mechanisms of near-wall turbulent structures. *J. Fluid Mech.* **287**, 317–348.

HOF, B., DE LOZAR, A., AVILA, M., T, X. & SCHNEIDER, T. M. 2010 Eliminating turbulence in spatially intermittent flows. *Science* **327**, 1491–1494.

HOLZNER, M., SONG, B., AVILA, M. & HOF, B. 2013 Lagrangian approach to laminar-turbulent interfaces. *J. Fluid Mech.* **723**, 140–162.

JIANG, X. Y., LEE, C. B., CHEN, X., SMITH, C. R. & LINDEN, P. F. 2020*a* Structure evolution at early stage of boundary-layer transition: simulation and experiment. *J. Fluid Mech.* **890**, A11.

JIANG, X. Y., LEE, C. B., SMITH, C. R., CHEN, J. W. & LINDEN, P. F. 2020*b* Experimental study on low-speed streaks in a turbulent boundary layer at low Reynolds number. *J. Fluid Mech.* **903**, A6.

KLOTZ, L., PAVLENKO, A. M. & WESFREID, J. E. 2021 Experimental measurements in plane Couette–Poiseuille flow: dynamics of the large-and small-scale flow. *J. Fluid Mech.* **912**, A24.

LINDGREN, E. R. 1957 The transition process and other phenomena in viscous flow. *Ark. Fys.* *12* **12**, 1–169.

323 LINDGREN, E. R. 1969 Propagation velocity of turbulent slugs and streaks in transition pipe
324   flow. *Phys. Fluids* **12**, 418.
325 MESEGUER, A. 2003 Streak breakdown instability in pipe Poiseuille flow. *Phys. Fluids* **15**, 1203–
326   1213.
327 MESEGUER, A. & TREFETHEN, L.N. 2003 Linearized pipe flow to Reynolds number 10^7.
328   *J. Comput. Phys.* **186**, 178–197.
329 NISHI, M., ÜNSAL, B., DURST, F. & BISWAS, G. 2008 Laminar-to-turbulent transition of pipe
330   flows through puffs and slugs. *J. Fluid Mech.* **614**, 425–446.
331 PEI, J., CHEN, J., SHE, Z.-S. & HUSSAIN, F. 2012 Model for propagation speed in turbulent
332   channel flows. *Phys. Rev. E* **86**, 046307.
333 RINALDI, E., CANTON, J. & SCHLATTER, P. 2019 The vanishing of strong turbulent fronts in
334   bent pipes. *J. Fluid Mech.* **866**, 487–502.
335 SCHOPPA, W. & HUSSAIN, F. 1998 Formation of near-wall streamwise vortices by streak
336   instability. *AIAA Paper* **98**, 3000.
337 SCHOPPA, W. & HUSSAIN, F. 2002 Coherent structure generation in near-wall turbulence.
338   *J. Fluid Mech.* **453**, 57–108.
339 SHAN, X., MA, B., ZHANG, Z. & NIEUWSTADT, F. T. M. 1999 Direct numerical simulation of
340   a puff and a slug in transitional cylindrical pipe flow. *J. Fluid Mech.* **387**, 39–60.
341 SHIMIZU, M. & KIDA, S. 2009 A driving mechanism of a turbulent puff in pipe flow. *Fluid Dyn.*
342   *Res.* **41**, 045501.
343 SONG, B., BARKLEY, D., HOF, B. & AVILA, M. 2017 Speed and structure of turbulent fronts
344   in pipe flow. *J. Fluid Mech.* **813**, 1045–1059.
345 SWEARINGEN, J. D. & BLACKWELDER, R. F. 1987 The growth and breakdown of streamwise
346   vortices in the presence of a wall. *J. Fluid Mech.* **182**, 255–290.
347 TAO, J. J., ECKHARDT, B. & XIONG, X. M. 2018 Extended localized structures and the onset
348   of turbulence in channel flow. *Phys. Rev. Fluids* **3**, 011902(R).
349 TUCKERMAN, L. S., CHANTRY, M. & BARKLEY, D. 2020 Patterns in wall bounded shear flows.
350   *Ann. Rev. Fluid Mech.* **52**, 343.
351 WALEFFE, F. 1997 On a self-sustaining process in shear flows. *Phys. Fluids* **9**, 883–900.
352 WANG, M. & GOLDENFELD, N. 2022 Stochastic model for quasi-one-dimensional transitional
353   turbulence with streamwise shear interactions. *Phys. Rev. Lett.* **129**, 034501.
354 WU, X. & MOIN, P. 2008 A direct numerical simulation study on the mean velocity
355   characteristics in turbulent pipe flow. *J. Fluid Mech.* **608**, 81–112.
356 WYGNANSKI, I. J. & CHAMPAGNE, F. H. 1973 On transition in a pipe. Part 1. The origin of
357   puffs and slugs and the flow in a turbulent slug. *J. Fluid Mech.* **59**, 281–335.
358 ZIKANOV, O. Y. 1996 On the instability of pipe Poiseuille flow. *Phys. Fluids* **8**, 2923.